Biogeosciences, 10, 3109–3125, 2013
www.biogeosciences.net/10/3109/2013/
doi:10.5194/bg-10-3109-2013

Biogeosciences Open Access

Implications of elevated CO_2 on pelagic carbon fluxes in an Arctic mesocosm study – an elemental mass balance approach

J. Czerny[1], K. G. Schulz[1,6], T. Boxhammer[1], R. G. J. Bellerby[2,3,4], J. Büdenbender[1], A. Engel[1], S. A. Krug[1], A. Ludwig[1], K. Nachtigall[1], G. Nondal[4], B. Niehoff[5], A. Silyakova[2], and U. Riebesell[1]

[1]GEOMAR Helmholtz Centre for Ocean Research Kiel, 24105 Kiel, Germany
[2]Bjerknes Centre for Climate Research, 5007 Bergen, Norway
[3]Geophysical Institute, University of Bergen, 5007 Bergen, Norway
[4]Norwegian Institute for Water Research (NIVA), 5006 Bergen, Norway
[5]Alfred Wegener Institute for Polar and Marine Research, 27515 Bremerhaven, Germany
[6]Centre for Coastal Biogeochemistry, Southern Cross University, Lismore, NSW 2480, Australia

Correspondence to: J. Czerny (jczerny@geomar.de)

Received: 31 July 2012 – Published in Biogeosciences Discuss.: 31 August 2012
Revised: 28 March 2013 – Accepted: 7 April 2013 – Published: 8 May 2013

Abstract. Recent studies on the impacts of ocean acidification on pelagic communities have identified changes in carbon to nutrient dynamics with related shifts in elemental stoichiometry. In principle, mesocosm experiments provide the opportunity of determining temporal dynamics of all relevant carbon and nutrient pools and, thus, calculating elemental budgets. In practice, attempts to budget mesocosm enclosures are often hampered by uncertainties in some of the measured pools and fluxes, in particular due to uncertainties in constraining air–sea gas exchange, particle sinking, and wall growth. In an Arctic mesocosm study on ocean acidification applying KOSMOS (Kiel Off-Shore Mesocosms for future Ocean Simulation), all relevant element pools and fluxes of carbon, nitrogen and phosphorus were measured, using an improved experimental design intended to narrow down the mentioned uncertainties. Water-column concentrations of particulate and dissolved organic and inorganic matter were determined daily. New approaches for quantitative estimates of material sinking to the bottom of the mesocosms and gas exchange in 48 h temporal resolution as well as estimates of wall growth were developed to close the gaps in element budgets. However, losses elements from the budgets into a sum of insufficiently determined pools were detected, and are principally unavoidable in mesocosm investigation. The comparison of variability patterns of all single measured datasets revealed analytic precision to be the main issue in determination of budgets. Uncertainties in dissolved organic carbon (DOC), nitrogen (DON) and particulate organic phosphorus (POP) were much higher than the summed error in determination of the same elements in all other pools. With estimates provided for all other major elemental pools, mass balance calculations could be used to infer the temporal development of DOC, DON and POP pools.

Future elevated pCO_2 was found to enhance net autotrophic community carbon uptake in two of the three experimental phases but did not significantly affect particle elemental composition. Enhanced carbon consumption appears to result in accumulation of dissolved organic carbon under nutrient-recycling summer conditions. This carbon overconsumption effect becomes evident from mass balance calculations, but was too small to be resolved by direct measurements of dissolved organic matter. Faster nutrient uptake by comparatively small algae at high CO_2 after nutrient addition resulted in reduced production rates under future ocean CO_2 conditions at the end of the experiment. This CO_2 mediated shift towards smaller phytoplankton and enhanced cycling of dissolved matter restricted the development of larger phytoplankton, thus pushing the system towards a retention type food chain with overall negative effects on export potential.

Published by Copernicus Publications on behalf of the European Geosciences Union.

1 Introduction

Increasing atmospheric CO_2 concentration is the major man-made geochemical perturbation characterising the anthropocene (Doney, 2010; Revelle and Suess, 1957). Atmospheric CO_2 partial pressure already increased by 40 % since the beginning of industrialisation, while rates of CO_2 emissions are continuing to increase beyond most modelled worst-case scenarios, e.g. SRES (Special Report on Emissions Scenarios) A1FI (Meehl et al., 2007; Friedlingstein et al., 2010). Correlations of increasing CO_2 concentrations to global warming are predictable and documented by current measurements as well as in the geological record (Hansen et al., 2006; Petit et al., 1999). About one third of the currently emitted CO_2 is dissolving in the world oceans, serving as a buffer for global climate change (Sabine et al., 2004). However, most of the absorbed CO_2 is accumulating in the surface ocean, separated from deep water masses by thermal stratification, which will further strengthen under global warming. In surface waters, ocean carbonation (increasing CO_2 concentrations) and consequential ocean acidification (decreasing pH) are affecting marine organisms, thereby modulating ecosystem functioning (Riebesell et al., 2009). A predominant geochemical function of the marine planktonic ecosystem is the formation of organic matter from dissolved CO_2. Sinking of this organic matter, transporting carbon across barriers of physical mixing into the ocean interior is referred to as the biological carbon pump (Sarmiento and Le Quéré, 1996; Volk and Hoffert, 1985). Increasing temperatures affect the ocean's function as a physical CO_2 sink, but acidification and carbonation are likely to impact also future biological carbon sequestration (Riebesell and Tortell, 2011; Gruber, 2011).

The Arctic Ocean plays a key role in sequestration of anthropogenic carbon for several reasons. From the physical perspective, high solubility of CO_2 in cold water leads to a high physical sequestration potential of anthropogenic CO_2 in areas of deep water formation. From the biological perspective, nutrient supply to the surface layer during winter deep mixing can promote pulses of high productivity with a large potential for carbon export via the biological pump (Lutz et al., 2007). Whether there is a net release or sequestration of atmospheric carbon depends on the carbon to nutrient ratio and sinking rate of the material exported after a mixing event. These properties are known to be highly variable, depending on food web structure. Deep sedimentation events in the Arctic Ocean may occur when fast sinking particles are formed, i.e. through coagulation of diatom blooms (Klaas and Archer, 2002) or by pteropods and their sticky nets (Bathmann et al., 1991). But efficient recycling of material by a surface layer retention food web may keep export at a low level (von Bodungen et al., 1995). Ocean warming and acidification are expected to impact ecosystems particularly in Arctic regions. Sea-surface warming will likely result in elevated primary production due to a reduction of sea ice cover and the shoaling of mixed layer depth in the light limited Arctic. Estimates for these effects of sea-surface warming are implemented in various global carbon flux models (Bopp et al., 2001; Sarmiento et al., 2004; Schmittner et al., 2008), whereas effects of changing seawater carbonate chemistry and pH on Arctic community export production are more difficult to quantify.

Ocean acidification and carbonation have the potential to directly affect ecosystem functioning in numerous ways. Of those, the adverse effect of future decreasing pH and carbonate ion concentrations on marine calcification is the most investigated mechanism (Riebesell, 2004; Fabry et al., 2008). Pteropods and foraminifera, the only calcifying organisms of significant relevance to the high Arctic pelagic ecosystem examined, were found to be very sensitive to ocean acidification (Comeau et al., 2009; Lombard et al., 2010; Lischka et al., 2011). Carbonation is also found to directly affect photoautotrophic carbon fixation of cultured marine phytoplankton and natural plankton assemblages (Riebesell and Tortell, 2011). In most studies, elevated CO_2 is reported to enhance carbon fixation, however, CO_2 affinity differs between different algal taxonomic groups (Reinfelder, 2011). In addition to effects of ocean carbonation on primary production, bacterial enzymatic rates were found to be directly affected by decreasing seawater pH (Piontek et al., 2010). Moreover, chemical speciation of potentially limiting micronutrients seems to be pH dependent in the range of projected ocean acidification (Millero et al., 2009).

Increased inorganic carbon consumption in response to elevated pCO_2 was already found in incubated natural plankton communities of the North Atlantic (Hein and Sand-Jensen, 1997) and in mesocosm studies in a Norwegian Fjord compiled by Riebesell et al. (2008). CO_2 induced overconsumption of carbon that was presumably exuded by phytoplankton cells in form of organic matter, which was measured as transparent exopolymer particles (TEP). The sticky carbon-rich TEP aggregated with other particles in the water column, thereby potentially increasing carbon export (Engel, 2002; Engel et al., 2004a). Enrichment of carbon relative to nitrogen in the exported matter would cause a substantial increase in the total amount of carbon sequestered in the future ocean (Oschlies, 2009).

This study investigates the response of a natural Arctic plankton community, including all trophic levels from bacteria to millimetre-sized zooplankton, to changes in seawater carbonate chemistry. Treatment levels ranged from ~ 180 µatm CO_2, as prevailing during the early summer situation in the beginning of the experiment, over present day and year 2100 atmospheric projections to extreme values of up to 1420 µatm CO_2. Using tracer gas exchange measurements and quantitative high resolution sediment sampling, we are able to present daily budget calculations for carbon, nitrogen, and phosphorus in all mesocosms. Mass balance calculations were used to crosscheck measured trends and to provide a quantitative evaluation of biogeochemical

fluxes. A "Pool X" representing the carbon not reproducibly measured on a daily basis will be discussed to evaluate the performance of the applied methods and to identify problematic measurement parameters. Those parameters (DOC, DON and POP) will be then estimated based on mass balance calculations. CO_2-induced changes in carbon fluxes within the water column, towards export and in exchange with the atmosphere are detected using correlation statistics. The presented dataset focuses on carbon fixation and export, but is however too unspecific to provide detailed insights into ecosystem functioning. Based on the presented mass balance, elemental cycling and export is discussed with reference to publications on the same experiment, putting biogeochemistry in the context of the observed plankton community composition.

2 Material and methods

2.1 Experimental set-up

Nine KOSMOS (Kiel Off-Shore Mesocosms for future Ocean Simulation) mesocosms were moored in the Kongsfjord, Svalbard (78°56.2′ N, 11°53.6′ E). The enclosures were cylindrical polyurethane bags 2 m in diameter, 17 m long and reaching ∼ 15 m deep into the water. The bags were supported by a stainless steel and glass fibre flotation frame and weighted at the bottom with steel rings closable with polycarbonate watertight shutters. The bags reaching 2 m above the water surface were open to the atmosphere. A spiked roof was mounted at the top to prevent birds from resting on the structures and introducing nutrients into the system (Fig. 1). The fjord water, enclosed by lowering of the bags on the 31 May 2010 (t-7), had a salinity of about 34. The mesocosms contained a natural plankton community, though larger plankton and nekton were excluded using a net (3mm mesh size) covering the upper and lower opening of the mesocosms during filling. After simultaneous watertight closure of the systems on t-5, flotation rings (Fig. 1) were released from the bottom shutters to buoy upwards, unfolding funnel-type sediment traps of 2 m height. This upper ring of the funnel was of the same diameter as the bag (2 m), therefore touching it on all sides. The rather tight fit of the funnel was chosen to minimise sediment losses at the sides but resulted in $\sim 4.5\,m^3$ of water below the funnel, which had only limited exchange with the bulk of enclosed water above the funnel. Depending on water/bag movement, water exchange between mesocosms and this "dead volume" happened on a timescale of days. Sediment lost into this dead volume was observed by divers to be very low (for calculated estimates see Table 1); nonetheless additions of dissolved substances (e.g. manipulations) to the water column had to mix with this dead volume before reliable budgets could be calculated. Pteropods of the species *Limacina helicina*, individually collected in the fjord, were added to each mesocosm (100, 20 and 70 individuals on day t4, t5 and t6, respectively). Most of them died within a few days in the tight gap between sediment funnel and mesocosm wall. Dead pteropods were picked from sediment samples or ended up in the dead volume. For more detail on the set-up see Riebesell et al. (2013) and find detailed information on abiotic conditions and standing stock succession of phytoplankton, dissolved and particulate matter in Schulz et al. (2013).

2.2 Manipulation

The water volume enclosed in flexible wall mesocosms can vary by some percent and was therefore determined using small additions of a calibrated NaCl solution as a tracer ($\sim 1\,mL\,L^{-1} = 0.2\,g\,L^{-1}$). Salinity measurements allowed calculation of the enclosed water volume of each individual mesocosm with uncertainties of less than 1 % (Czerny et al., 2013a). Measurements were performed twice, on t-4 and t4, because of considerable uncertainties in salinity measured before the first tracer addition on t-4. Measured volumes were consulted to plan further manipulation steps and to calculate elemental budgets. From t-1 to t4, CO_2 enriched filtered seawater solution was added to achieve eight CO_2 treatments between 185 and 1420 µatm CO_2, spanning a pH gradient from 8.31 to 7.51 (measured after mixing with the dead volume on t8). The two ∼ 180 µatm CO_2 "control" mesocosms were undersaturated with respect to atmospheric CO_2 at the time the mesocosms were deployed and were blank manipulated using 55 µm filtered fjord water. All mesocosms were enriched with N_2O as a gas exchange tracer to a final concentration of $\sim 50\,nmol\,kg^{-1}$ on t4, when the second salt addition was performed. Before sampling on t13, a seawater-based mixed nutrient solution, calculated for the volumes of each single mesocosm, was added to establish equal concentrations of NO_3^- ($5\,\mu mol\,kg^{-1}$), PO_4^{3-} ($0.31\,\mu mol\,kg^{-1}$) and SiO_3^{2-} ($2.5\,\mu mol\,kg^{-1}$) in all mesocosms. All additions were performed using the "Spider" injection system (Fig. 1a). For a more detailed description of the mesocosm manipulation technique see Riebesell et al. (2013). And for a description of inorganic nutrient dynamics see Schulz et al. (2013).

2.3 Sampling

The entire experiment from filling (t-7) to the last sampling of the mesocosms (t31) lasted 39 days. Sampling started at t-3, two days prior to the beginning of the CO_2 manipulation and lasted until t30 for most variables presented here. Daily water sampling for dissolved and particulate matter (representing total inorganic carbon (CT), dissolved inorganic nitrogen (DIN) and phosphorus (DIP), dissolved organic carbon (DOC), nitrogen (DON) and phosphorus (DOP), as well as particulate carbon (PC), organic nitrogen (PON) and phosphorus (POP)) was between 09:00 and 11:00 LT (local time) from boats. Samples were taken using 5 L depth-integrating

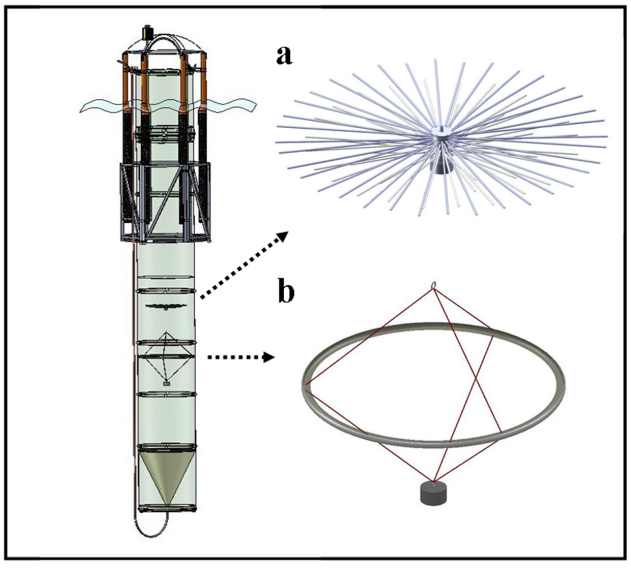

Fig. 1. Sketch of one of the nine experimental units. Total view of the mesocosm with **(a)** manipulation device "Spider" and **(b)** wall brush.

water samplers (IWS, Hydrobios, Kiel, Germany) that delivered one mixed sample from the upper 12 m, representing total water-column inventories. Sampling depth was restricted to 12 m to prevent dispersion of sediment from the 2 m-high collecting funnel at the bottom of the mesocosms. Immediately after water collection, gas samples for N_2O and carbonate chemistry (CT and total alkalinity (TAlk)) were collected directly from the sampler into gas-tight bottles. The rest of the water was transferred into 20 L polyethylene carboys using a silicon tube. Carboys were transported into the lab, screening them from sunlight using black plastic foil. Samples for dissolved and particulate matter were subsampled from carboys. Vertical (0–12 m depth) Apstein net hauls (opening Ø 17 cm, mesh size 55 µm) were performed to determine zooplankton abundance and biomass. To minimise effects on zooplankton density, samples were taken only once per week (days t-2, t2, t11, t18, t24 and t30). For more details see Niehoff et al. (2013).

Sediment was sampled every other day using silicone tubes (10 mm inner diameter) connecting the tips of the sediment funnels to the water surface (Fig. 1). Sediment dispersed in approximately 3 L of water was drawn from the silicone tube into a glass bottle under low vacuum pressure. After gravimetric determination of the sediment-water volume sampled, 20 to 30 mL sub-samples for microscopic inspection were taken with a pipette from the stirred bottles. For bulk chemical analyses (PC, PON, POP and biogenic silica (BSi)), particles were concentrated by settling and centrifugation, and the resulting compact sediment pellets were frozen at −80 °C.

2.4 Measurement procedures

Aliquots of water samples for analyses of chlorophyll *a* (Chl *a*; 250–500 mL) , PC, PON and POP (400–500 mL) were filtered under low vacuum (200mbar) on glass fibre filters (Whatman GF/F 25 mm Ø, pre-combusted at 450 °C for 5h) and stored frozen at −20 °C. Chl *a* was determined fluorometrically according to Welschmeyer (1994) using a Turner fluorometer 10-AU (Turner BioSystems). Quantification of PC and PON was carried out using an elemental analyser (EuroVektor EA) according to Sharp (1974). POP and BSi was determined following the method by Hansen and Koroleff in Grasshoff et al. (1983). For POP this method was modified to the measurement of samples on glass fibre filters. Here, particulate matter was completely oxidised by heating the filters in 50 mL glass bottles with 40 mL of purified water and the reagent Oxisolv (Merck) in a pressure cooker. Solutions were measured colorimetrically on a Hitachi U 2000 spectrophotometer. DOC, DON and DOP were determined from filtered (Whatman GF/F 25 mm Ø, pre-combusted at 450 °C for 5 h) water samples. DOC was analysed on a Shimadzu TOC_{VCN} using the HTCO (high-temperature catalytic oxidation) method (Qian and Mopper, 1996); for details see Engel et al. (2013). DON and DOP were oxidised as described for POP and subsequently measured as inorganic nutrients, for nitrate (NO_3^-), nitrite (NO_2^-) and phosphate (PO_4^{3-}) according to Hansen and Koroleff (1999), and for ammonia (NH_4^+) according to Holmes et al. (1999). The sum of NO_3^-, NO_2^- and NH_4^+ is presented as dissolved inorganic nitrogen (DIN). For a more detailed description of particulate matter (POM) and dissolved organic matter (DOM) and inorganic matter (DIM) analyses see Schulz et al. (2013). CT was determined via coulometric titration using a SOMMA (Single Operator Multiparameter Metabolic Analyser) system, and TAlk via potentiometric titration (Dickson, 1981). CO_2 concentrations, partial pressures and pH (total scale) were calculated from CT and TAlk measurements with the program CO2SYS by Lewis and Wallace (1998). For more details on carbonate chemistry see Bellerby et al. (2012).

Frozen sediment pellets were freeze dried at a pressure of ∼ 50 mbar for 1–2 days without additional heat input until room temperature was reached. Subsequently, the dried sediment was ground in a stainless steel ball mill at low temperatures using liquid nitrogen to cool the sample before grinding. Sub-samples adjusted to the analytic measurement range (5–10 mg) were weighed on a precision scale. Analyses of particulate matter were performed as described above for PC, PON, POP and BSi on filters. 20 to 30 mL sub-samples of the sediment suspension, as well as samples from vertical net hauls were analysed for zooplankton composition, abundance and biomass under a dissecting microscope. At the same time, sediment samples were also inspected for general composition (detritus and phytoplankton). Zooplankton was sorted into tin cups for bulk carbon and nitrogen analyses as

described above for water-column PC and PON. For more details on zooplankton analyses see Niehoff et al. (2013).

2.5 CO_2 gas exchange estimate

Daily air–sea gas exchange velocities (k) were estimated using N_2O as a gas tracer. Calculations were based on fitted concentration decrease inside the mesocosm in relation to calculated equilibrium concentrations estimated using water T/S and atmospheric N_2O concentrations monitored on Zeppelin Mountain ($\sim$ 4 km distance from the experimental site). Daily CO_2 fluxes were calculated using k (adapted to CO_2 using published Schmidt numbers) together with CO_2 air–sea diffusion gradients. CO_2 gradients were derived from bulk aquatic CO_2 concentrations calculated from CT and AT as well as estimated using bulk water T/S and atmospheric CO_2 concentrations recorded on Zeppelin Mountain. Corrections for chemical enhancement by Hoover and Berkshire (1969) were applied. For a detailed discussion on gas exchange measurements in mesocosms including complete references on used constants see Czerny et al. (2013b). Zeppelin Mountain atmospheric data were provided by Thomas Conway from the NOAA Carbon Cycles Gases Group in Boulder, US, and Johan Ström from ITM (Department of Applied Environmental Science), Stockholm University, Sweden; atmospheric N_2O and CO_2 measurements, respectively.

2.6 Wall growth estimate

After sampling on the last day of the experiment (t30), a special brush (Fig. 1b) was used to mechanically remove and suspend biomass growing on the inner surface of the mesocosm bag as described in Riebesell et al. (2013). The detached biomass was then quantified by POM measurements of the water column before and right after brushing as described above.

2.7 Data presentation

Budget calculations for carbon (C), nitrogen (N) and phosphorus (P) are based on changes in pool sizes over time (Δpool) relative to a reference point in time. The addition of CO_2 enriched seawater caused major changes in the CT budget that could only be precisely quantified by direct measurements of CT inside the mesocosms. The earliest reference points for CT budgets were measured after complete mixing of the water column above and below the sediment traps. In the high CO_2 mesocosms this took until t8, while CT values were found to be stable in the non-manipulated control and in some low CO_2 mesocosms earlier. N and P budgets were calculated starting on t13, after inorganic nutrients were added. As a reference value for ΔDIN and ΔDIP from t13 onwards, concentrations measured on t12 plus the known amounts of added inorganic nutrients were used. This particular reference point was chosen because, in this way, budget calculation could be started on the day of nutrient addition, e.g. before the added nutrients were fully mixed into the dead volume below the sediment traps (see Sect. 2.1). For dissolved and particulate organic matter, starting values (t0, t8, t13, t20) for the analysed phases were obtained by averaging measured concentrations of the respective days with those of the days before and after. As measurement precision for inorganic matter is much higher than for organic material, averaging over three consecutive days was not needed and the concentrations of dissolved inorganic pools measured on the reference days were used as starting values.

Measured changes in inorganic matter that cannot be accounted for by the combined changes in pools of dissolved and particulate organic matter, cumulative gas exchange and sedimentation were assigned as "Pool X", representing a combination of measurement errors and the following pools unaccounted for in daily sampling: (1) a small amount of sedimented material accumulated in the space surrounding the sediment trap (dead volume) that could not be sampled. (2) A biofilm growing on the mesocosm walls became visible towards the end of the experiment. The size of this pool was estimated from water-column measurements taken immediately before and after brushing the mesocosm walls. (3) Fast-swimming zooplankton such as copepods were not quantitatively sampled with the depth-integrating sampler and are therefore not adequately represented in PC/PON/POP measurements. Biomass of zooplankton larger than 55 µm was estimated by weekly Apstein net hauls. Estimates for these three contributors to Pool X within the three phases of the experiment are based on theoretical considerations combined with available data on wall growth, zooplankton, and sediments (Table 1). Due to a rather constant elemental composition of particulate matter close to Redfield ratios of 106/16/1, those uncertainties in nitrogen and phosphorus are proportionally smaller than presented uncertainties in carbon (data not shown).

Corrections for the effect of water evaporation on dissolved and particulate matter concentrations as well as corrections for the effect of sampling-derived volume decrease on the calculation of air–sea and sediment fluxes were not included to keep calculations traceable. With a range of $\sim$ 0.2 % and $\sim$ 1 %, respectively, over the whole experiment, corrections are below the detection limit of most of the applied methods. Moreover, the effects of small changes in water volume would be identical in all mesocosms.

Changes in Pool X ($\Delta X_{C/N/P}$) were calculated for the three phases of the experiment as the summed amount of changes in all major pools as:

$$\Delta X_C = \Delta CT + \Delta GX + \Delta PC + \Delta DOC + \Delta Sed_C, \quad (1)$$

$$\Delta X_N = \Delta DIN + \Delta PON + \Delta DON + \Delta Sed_N, \quad (2)$$

$$\Delta X_P = \Delta DIP + \Delta POP + \Delta DOP + \Delta Sed_P. \quad (3)$$

Table 1. Estimates for the contribution of undetermined carbon pools (or not daily determined pools) to Pool X or ΔDOC_{calc}. Sediment losses were estimated on the basis of the ratio of areas of funnel opening relative to the gap around the funnel and the average cumulative sediment trapped during each phase. The area from which particles would collect in the gap was estimated as radius × length of the sediment trap flotation ring. Copepod biomass changes were estimated from average counts and carbon content determined from weekly net hauls. The depicted value was calculated assuming copepods were not at all represented in the particulate carbon measurements from water samples. Wall growth for phases II and III (after nutrient addition) was estimated, assuming exponential growth of the wall-grown carbon measured on t30 ($8.31 \pm 3.1\,\mu mol\,kg^{-1}$) at rates of 1 to 0.3 per day (Hagseth et al., 1992). "Maximum contribution of undetermined pools" depicts the sum of estimated mean changes within the three listed pools plus one standard deviation, or in the case of wall growth, the largest estimate.

Phase	I [$\mu mol\,kg^{-1}$]	II [$\mu mol\,kg^{-1}$]	III [$\mu mol\,kg^{-1}$]
Sediment lost into dead volume	0.046 ± 0.007	0.10 ± 0.015	0.17 ± 0.063
Copepod biomass changes	$0.0 + 0.11$	0.26 ± 0.43	1.11 ± 0.78
Wall growth	none	0.081 to 0.82	1.0 to 3.4
Maximum contribution of undetermined pools	0.12	1.63	5.52
Observed range of ΔDOC_{calc} on the last day of the phase	−0.93 to 11.09	−7.02 to 8.81	19.32 to 30.5

With ΔCT = change in total inorganic carbon concentrations, ΔGX = cumulative exchange of carbon with the atmosphere (flux in = negative/out = positive), ΔPC = change in total particulate carbon concentrations, ΔDOC = change in dissolved organic carbon concentrations, ΔSed = cumulative amounts of the respective element found in the sediment trap, ΔDIN = change in dissolved inorganic nitrogen concentrations, ΔPON = change in particulate organic nitrogen concentrations, ΔDON = change in dissolved organic nitrogen concentrations, ΔDIP = change in dissolved inorganic phosphorus concentrations, ΔPOP = change in particulate organic phosphorus concentrations, ΔDOP = change in dissolved organic phosphorus concentrations.

Pool X should be ideally zero as changes in one of its components should always be balanced by changes in one or several others. To trace back the source of changes in Pool X, regression analyses were performed, thus testing the degree of variance in all daily Pool X within each phase to be explained by changes in each of the single components on corresponding days (Fig. 2, Table 2). In this way, unexplained variability in measured concentrations of DOC, DON and POP were found to explain most of the variability in Pool X for carbon, nitrogen and phosphorus, respectively. Therefore mass balance calculations were used to estimate possible changes in DOC, DON and POP on the basis of all other budget components. Those estimates are presented as DOC_{calc}, DON_{calc} and POP_{calc}. Bias in these estimates, composed of summed measurement uncertainties and errors in the combined variables as well as undetermined pools (Table 1), is considerably lower than measurement errors in DOC, DON and POP.

Thus, estimates of DOC_{calc}, DON_{calc} and POP_{calc} were calculated using mass balances according to the following equations:

$$\Delta DOC_{calc} = \Delta CT + \Delta GX + \Delta PC + \Delta Sed_C, \quad (4)$$

$$\Delta DON_{calc} = \Delta DIN + \Delta PON + \Delta Sed_N, \quad (5)$$

$$\Delta POP_{calc} = \Delta DIP + \Delta DOP + \Delta Sed_P. \quad (6)$$

As sediment traps were sampled every other day, measured values were linearly interpolated for days in between. Also missing data points of other parameters were linearly interpolated between preceding and subsequent measurements. This applies for DON and DOP of all mesocosms on t16 and t19 and for 8 single data points of DOC.

2.8 Statistics

The set-up with 8 different CO_2 treatment levels and no replication of treated mesocosms was designed for regression analyses. Delta values of all tested phases are calculated using the first day of the respective phase as a reference point. Means of changes in measurement parameters (Δvalues) of single mesocosms during the three phases of the experiment were plotted against mean pCO_2 in the mesocosms during that specific phase. The null hypothesis that the overall slope is zero and that there is no linear relationship between treatment pCO_2 and mean Δ values was statistically tested with an F test. Data satisfied assumptions for normal distribution, as confirmed by a Shapiro–Wilk test. Analyses were performed using the program Statistica 6.0 (StatSoft Inc., Tulsa, USA). The same statistical procedure was applied to regression of Pool X to single budget components.

Table 2. Linear regression of daily Pool X of all mesocosms during each phase versus corresponding budget components (see Fig. 2). Coefficients of determination depict the share of variances in daily Pool X explained by variances in the datasets it is based on.

Regression of Pool X versus		ΔPC	ΔDOC	ΔCT	ΔGX	Sed
Phase I	r^2	0.01	0.85	0.01	0.00	0.03
	p	0.49	0.00	0.51	0.69	0.27
Phase II	r^2	0.00	0.90	0.11	0.09	0.10
	p	0.89	0.00	0.01	0.02	0.01
Phase III	r^2	0.08	0.51	0.24	0.08	0.22
	p	0.03	0.00	0.00	0.03	0.00

3 Results

3.1 Chlorophyll *a* and the analysed phases of the experiment

The experiment can be divided into three phases of autotrophic bloom development. An increase in Chl *a* (Fig. 3) started in all mesocosms already during CO_2 manipulation and peaked on t7. A CO_2 effect on Chl *a* concentrations during phase I was not observed. After nutrient addition (t13), there was a lag phase of 2 to 3 days until Chl *a* started to increase. Phase I carbon budget-calculation starts on t8, just after the phase I peak, and is thus describing processes during the bloom decay until t15. During phase II, from t13 onwards, large parts of added inorganic nutrients were consumed and budgets for C, N and P were calculated for build-up and decay of the second bloom peak until t20. Here, the Chl *a* peak of the high CO_2 treatments was higher than the one at intermediate and low CO_2 levels. During phase III, starting on t20, Chl *a* at low and intermediate CO_2 started to increase exponentially, reaching maximum concentrations on t27 and declining thereafter. In contrast, at high pCO_2 Chl *a* increased more slowly, not reaching peak values until the end of the experiment.

Maximal Chl *a* concentrations of $\sim 3\,\mu g\,L^{-1}$ during the course of the experiment are rather low considering the $5\,\mu mol\,kg^{-1}$ NO_3^- and $0.32\,\mu mol\,kg^{-1}$ PO_4^{3-} added. Chl *a* concentrations were transformed into estimates of organic carbon for the autotrophic community using Chl *a* to carbon ratios by Li et al. (2010), with $0.02\,g\,Chl\,a\,g\,C^{-1}$ for a phytoplankton community with low contribution of diatoms. Transformation reveals that the contribution of photoautotrophic biomass (up to $15\,\mu mol\,kg^{-1}\,C$) to the standing stock of particulate carbon, PC, (up to $40\,\mu mol\,kg^{-1}$) was rather low.

3.2 Carbon budget of the replicated control treatment

In Fig. 4 carbon pools of the untreated control mesocosms are plotted over the entire period of the experiment. The bloom development as displayed in Chl *a* (Fig. 3) is mirrored by build-up of ΔPC, while cumulative sedimentation of this

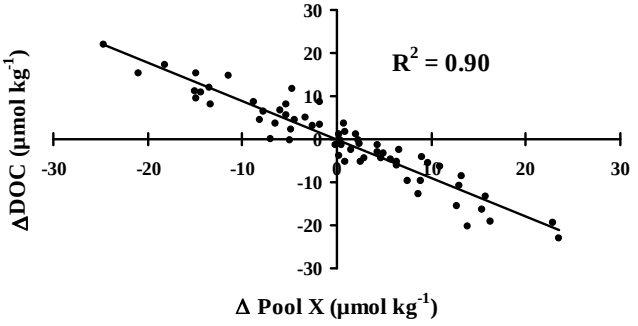

Fig. 2. Linear regression of changes in all daily total Pool X (ΣΔPC, ΔDOC, ΔCT, ΔSed, ΔGX) estimates within phase II to corresponding changes in measured DOC on the same days can be used to identify measured quantities of DOC to be unrealistic. Regression results of total Pool X to other carbon pools are given within Table 2.

biomass was rather low (Fig. 4a). Until t8, autotrophic uptake of inorganic carbon resulted in a simultaneous decrease of ΔCT, which was partly compensated by in-gassing of CO_2 from the atmosphere. Hereafter biomass decreased and PC was partly respired back into the CT pool, sedimenting out or being released as DOC_{calc}. Three days after the addition of inorganic nutrients (t16 up to t19), ΔPC build up combined with sedimentation was not leading to changes in ΔCT but was compensated by CO_2 entering the mesocosms from the atmosphere. During the first 19 days, the sum of particulate carbon produced in the control mesocosms roughly equalled the sum of inorganic carbon consumed, indicated by DOC_{calc} approaching zero during this period. Measured DOC values are included in Fig. 4b. Apparently, day-to-day variability in this dataset is much larger than the amount of carbon potentially available for the formation of DOC. This is evident from the sum of other measured carbon species shown as DOC_{calc} in Fig. 4a. Parallel variations of Pool X to DOC data (Figs. 2, 4b) identify measurement results to be unrealistic.

As shown in Fig. 4c, the temporal development of DOC_{calc} in the two control treatments was very similar. Variability of DOC_{calc} during most of the experimental time was relatively small (DOC_{calc} was on average $-0.43 \pm 2.7\,\mu mol\,kg^{-1}$ for

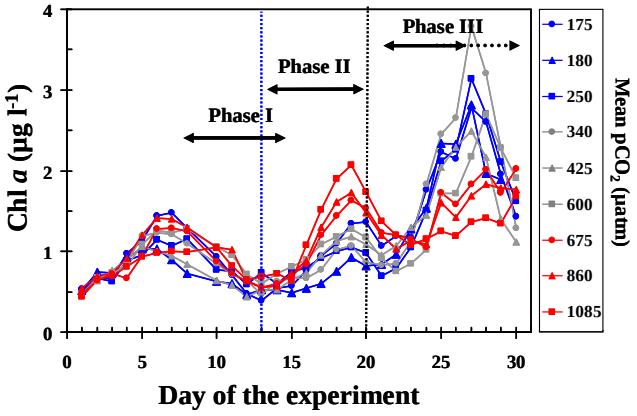

Fig. 3. Development of chlorophyll *a* concentrations during the course of the experiment. CO_2 partial pressures given in the figure legend are mean values for the experiment (day 8–26). High pCO_2 is denoted in red, intermediate in grey and low levels in blue. Within these categories, circles symbolise the lowest, triangles intermediate and squares the highest treatment pCO_2 level. The blue dashed line marks the nutrient addition (t13) at the end of phase I. The black dashed line denotes the end of phase II comprising the second bloom peak, phase III corresponds to the third bloom until the end of measurements. Arrows depict time periods used for statistical analyses.

the two controls until t19). Bias of DOC_{calc} estimates given in Table 1 could have caused a gradual increase in the DOC_{calc} of maximum 1.8 µmol kg^{-1} for this period. From t19 to t27, a phytoplankton bloom developed in the mesocosms, extensively consuming inorganic carbon. Increasing ΔPC values and cumulative sedimentation did not balance the sum of 44 µmol kg^{-1} CT taken up from the dissolved pool plus the CO_2 entering from the atmosphere (Fig. 4a). It therefore required 19 µmol kg^{-1} DOC_{calc} to close the carbon budget on t27. Within this period, biomass growing attached to the walls became visible and was estimated to account for 8.3 ± 3.1 µmol kg^{-1} of Pool X on t30 averaged over all mesocosms. This biomass was extrapolated back to the two nutrient-replete phases of the experiment based on assumed exponential growth at rates between 0.3 and 1.0, typical for ice algae communities (Hagseth et al., 1992). Even at the rather low growth rates, most of the wall grown biomass developed within the last few days before measurement, thus contributed shares to community biomass were negligible during phase I and II and moderate during phase III (Table 1). It has to be therefore assumed that carbon missing from the budget is largely dissolved organic carbon shown as DOC_{calc}. Only for phase III DOC_{calc} should be interpreted with caution. On the last sampling day (t27) undetermined pools (mainly wall growth) might have been contributing up to 5.5 of the 19 µmol kg^{-1} DOC_{calc}. Visual inspections by divers indicated that large parts of wall growth were removed by the brushing technique, but measurements most likely underestimated wall growth.

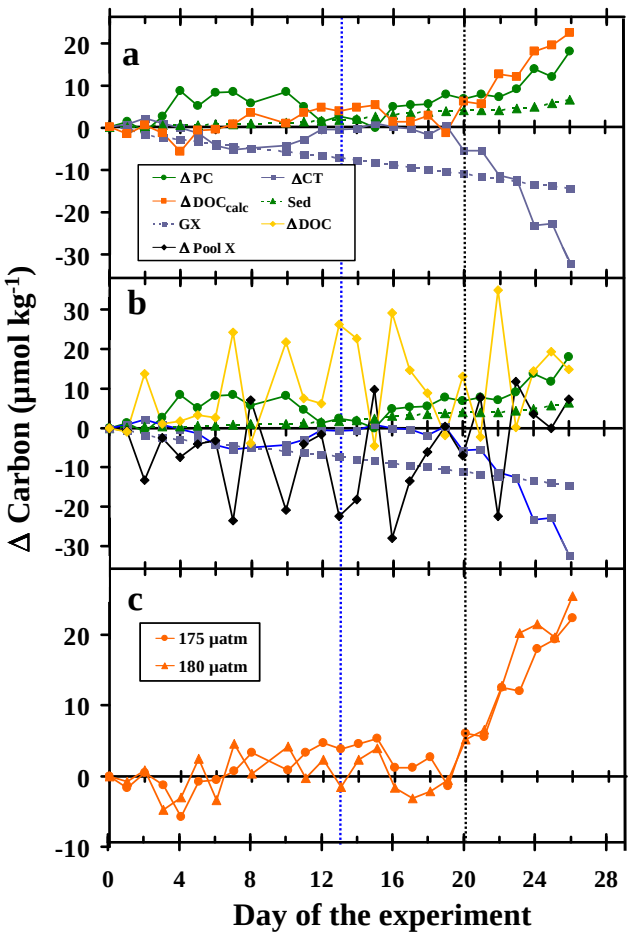

Fig. 4. Temporal development of carbon pools in the control treatment. **(a)** shows daily measured differences in particulate carbon (ΔPC), total inorganic carbon (ΔCT), dissolved organic carbon calculated from mass balance (DOC_{calc}), cumulative sedimented carbon (Sed) and CO_2 gas exchange (GX) relative to day zero for the lowest CO_2 treatment (175 µatm). In **(b)**, measured changes in dissolved organic carbon (ΔDOC) and Pool X (the carbon fraction that cannot be accounted for by changes in combined daily measured pools) are included. **(c)** compares DOC_{calc} of the 175 µatm treatment with DOC_{calc} of the second control mesocosm (180 µatm). The black dashed line denotes the end of phase II comprising the second bloom peak; phase III corresponds to the third bloom until the end of measurements.

3.3 CO_2 effects on carbon budgets

Changes in inorganic carbon concentrations between t8 and t27 (Fig. 5a) are correlated to CO_2 levels with the highest CO_2 treatment showing the strongest decrease in CT. At high pCO_2 the decrease was rather linear over time, whereas there was only a minor change in CT concentrations in the low CO_2 treatments during the first 12 days of this period. Most of these CO_2-related differences were caused by gas exchange with the atmosphere. One third (24 µmol kg^{-1}) of the CT decrease at the highest CO_2 over the whole

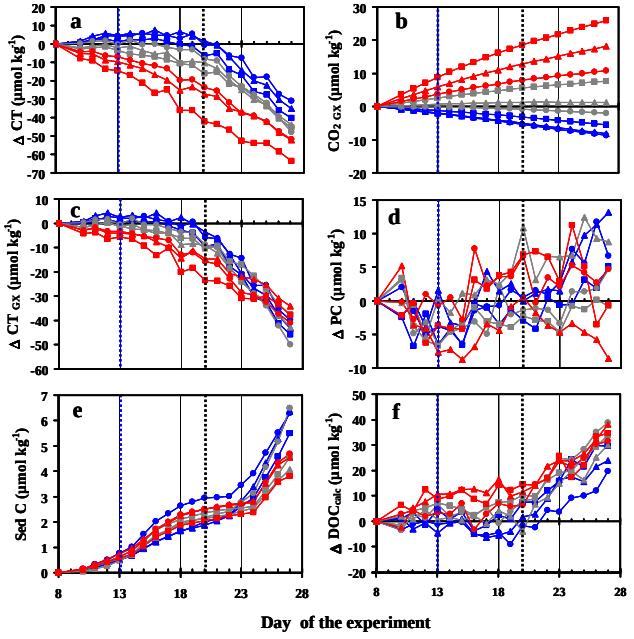

Fig. 5. Temporal development of carbon pools in all treatments relative to day 8. Changes in dissolved inorganic carbon (ΔCT) **(a)** corrected for gas exchange $CO_{2\,GX}$ **(b)** can be used to calculate biologically mediated changes in inorganic carbon concentrations (ΔCT_{GX}) **(c)**. This production estimate together with changes in particulate carbon (ΔPC) **(d)** and cumulative sedimentation of particulate carbon (Sed) **(e)** were used to estimate dissolved organic carbon from mass balance Δ DOC_{calc} **(f)**. CO_2 treatment levels and vertical dashed lines are coded as described for Fig. 3.

experiment can be attributed to outgassing, whereas about 25 % (10 µmol kg^{-1}) of the carbon consumed in the lowest CO_2 treatments entered from the atmosphere (Fig. 5b). The gas exchange corrected variation of ΔCT (Fig. 5c), ΔCT_{GX} is an approximation for biological net inorganic carbon fixation, as calcification was negligible during the experiment (Silyakova et al., 2012). Approximately equal amounts of inorganic carbon were consumed biologically in all treatments between t8 and t27. However, uptake rates often strongly differed among CO_2 treatments. CT was taken up immediately and rather continuously at high CO_2. At low CO_2, there was a considerable lag phase until t20, but then net uptake rates exceeded rates at high CO_2, so that all treatments ended up with similar uptake at the end of phase III. Overall, ΔPC build-up calculated from t8, with maximal 10 µmol kg^{-1} (Fig. 5d), was rather small compared to net carbon uptake ΔCT_{GX} of ∼ 40 µmol kg^{-1}. Cumulative sedimentation can only account for half as much as ΔPC build-up (up to 5 µmol kg^{-1}, Fig. 5e). As the build-up of both measured particulate carbon species (ΔPC and sediment) cannot explain the measured drawdown in ΔCT_{GX}, ΔDOC_{calc} is accumulating over time (Fig. 5f).

3.4 Phase I

By separating the budget into three phases of the experiment, changes in elemental pools in the nine mesocosms can be directly compared using regression analyses.

Because inorganic nutrients were low at the beginning of phase I, there was no apparent uptake and inorganic nutrient budgets were thus not calculated. However, ΔCT_{GX} (Fig. 6a) showed a relatively strong decrease of inorganic carbon at high CO_2 compared to net heterotrophic production at low CO_2. This highly significant CO_2 effect on carbon uptake was not reflected in particulate carbon accumulation (Fig. 6b, Table 3). ΔPC was decreasing from the t8 bloom peak, while sedimentation was equally low in all treatments. This translates into a significant positive correlation of ΔDOC_{calc} to CO_2 in phase I (Table 3), causing an offset towards elevated ΔDOC_{calc} at high CO_2 that persisted over most of the experimental time (Fig. 5f).

3.5 Phase II

During phase II, dissolved inorganic matter (DIM) concentrations, comprising inorganic carbon (Fig. 6e) together with inorganic nutrients, decreased significantly stronger at high CO_2 (Table 3). Although statistical tests could not detect a significant CO_2-related increase in all pools of dissolved and particulate organic matter, significant positive trends in Chl *a* (Fig. 3), ΔPON, ΔDOP and ΔDOC_{calc} (Fig. 6h, Table 3) suggest a general positive effect of CO_2 on phytoplankton production during phase II. Mass balance indicates that surplus carbon taken up at high CO_2 accumulated in the dissolved organic pool (ΔDOC_{calc}), while nitrogen remained mainly in the particulate fraction and phosphorus was almost equally partitioned between both the particulate and dissolved organic pool (Table 3). The small sedimentation event peaking on t16 can be mainly allocated to Cirripedia larvae migrating into the sediment trap (Figs. 7a, 6g). The settling of these meroplanktonic larvae decreased metazooplankton biomass by 40–60 % (from overall average 5.0 ± 1.8 to 3.1 ± 1.1 µmol kg^{-1}) over the course of the experiment, thereby contributing ∼ 60 % to the export flux during phases I and II (see also Niehoff et al., 2013). A sedimentation event caused by sticky nets of pteropods introduced into the mesocosm during phase I was not detected. The fairly large dead individuals were excluded from the sediment samples.

3.6 Phase III

In phase III, CO_2-related trends in dissolved inorganic matter uptake rates of phase II are reversed. Significantly more inorganic carbon was consumed at low CO_2 (Fig. 6i), resulting in significantly stronger build-up of PC (Fig. 6j) and export of this material (Fig. 6k). Trends in inorganic carbon uptake during phase III were parallel to trends in uptake of

Table 3. Results of F tests (regression analyses) for CO_2 dependent changes in pool sizes of C, N and P during the three phases of the experiment. Analysed delta values for each phase are calculated using the first day of the respective phase as a reference point. Mean delta concentrations of the elements in particulate organic (POM), dissolved inorganic (DIM) and dissolved organic matter (DOM) as well as sediments (Sed.) and pools calculated by mass balance (DOC_{calc} DON_{calc} POP_{calc}) were plotted against mean CO_2 concentrations during the phase. Significant trends ($p < 0.05$) are marked grey. Direction (Dir) of trends are given for correlations $p < 0.1$. "Neg." stands for negative correlation to pCO_2 and would for example mark a significantly stronger decrease in dissolved inorganic matter (DIM) with increasing pCO_2, while "Pos." stands for positive correlation to pCO_2 and could therefore mark significantly increasing concentrations, for example, POM with increasing pCO_2.

Testet period		ΔPOM			ΔDIM			ΔDOM			Sed.			ΔOM_{calc}		
		r^2	p	Dir	r^2	p	Dir	r^2	p	Dir	r^2	p	Dir	r^2	p	Dir
Phase	Carbon													DOC_{calc}		
I	T8–T15	0.01	0.78	–	0.98	< 0.00	Neg.	0.42	0.06	Pos.	0.02	0.75	–	0.96	< 0.00	Pos.
	Carbon													DOC_{calc}		
	T14-T21	0.27	0.15	–	0.92	< 0.00	Neg.	0.01	0.77	–	0.00	0.92	–	0.66	0.01	Pos.
Phase	Nitrogen													DON_{calc}		
II	T14–T21	0.52	0.03	Pos.	0.87	< 0.00	Neg.	0.25	0.17	–	0.02	0.69	–	0.07	0.50	–
	Phosphorus													POP_{calc}		
	T14–T21	0.35	0.10	–	0.93	< 0.00	Neg.	0.54	0.02	Pos.	0.02	0.71	–	0.13	0.34	–
	Carbon													DOC_{calc}		
	T21–T27	0.86	< 0.00	Neg.	0.85	< 0.00	Pos.	0.07	0.49	–	0.65	0.01	Neg.	0.35	0.09	Neg.
Phase	Nitrogen													DON_{calc}		
III	T21–T30	0.83	< 0.00	Neg.	0.89	< 0.00	Pos.	0.13	0.35	–	0.63	0.01	Neg.	0.25	0.17	–
	Phosphorus													POP_{calc}		
	T21–T30	0.31	0.12	–	0.94	< 0.00	Pos.	0.15	0.31	–	0.64	0.01	Neg.	0.47	0.04	Neg.

inorganic nutrients (Table 3). As inorganic N and P were supplied in the beginning of phase II in equal concentrations (5 µmol kg^{-1} DIN, 0.32 µmol kg^{-1} DIP), stronger uptake at high CO_2 during phase II resulted in lowered concentrations of the limiting nutrients during phase III. On t20, concentrations of $\sim$ 3.5 µmol kg^{-1} DIN and $\sim$ 0.2 µmol kg^{-1} DIP were available in the control treatments, but only approximately half of this amount in the highest CO_2 treatment (1.76 and 0.10 µmol kg^{-1} DIN and DIP, respectively). DIN and DIP were depleted in all mesocosms at about day t28. Uptake rates were considerably faster in the still relatively nutrient-replete low CO_2 treatments. On the last days of the experiment, net community production at low CO_2 exceeded all rates observed before during this experiment. CO_2-related trends in ΔPC, ΔPON and especially in export of C, N and P could be clearly detected. Changes in nearly all of the particulate pools showed highly significant negative correlations to treatment pCO_2 (Table 3).

DOC_{calc} (Fig. 6l) was steadily increasing until day 27 in all CO_2 treatments. Major parts of the nutrients added on t13 accumulated in those pools determined by mass balance until the end of the experiment on t30 (averaged $\sim$ 55 % in DON_{calc} and 74 % in POP_{calc}). Whereas 16 % of added N and 32 % of added P was measured as wall growth on t30 on average over all mesocosms. A CO_2 effect on wall growth is neither indicated by direct measurements on t30 nor by CO_2 correlations of DOC_{calc}, DON_{calc} or POP_{calc}, to which it was contributing during phase III.

3.7 Stoichiometry of particulate matter

Elemental ratios of water-column particulate matter were always close to Redfield ratios (Fig. 8). CO_2 or nutrient manipulation did not cause strong changes in elemental composition of particulate matter. C/N and N/P ratios of material sampled from the sediment traps were generally similar to ratios obtained for water-column particulate matter, with mean N/P ratios of the sediment slightly higher than respective values from the water column. During the last days (t27–t30) of the experiment, C/N ratios of water-column particulate matter increased in all mesocosms (Fig. 8a). This increase was significantly stronger for the low CO_2 treatments. The same general increase was observed in the sediment, but here C/N started to rise already on t24, reaching higher maximum values than in the water column (Fig. 8b). Diatom aggregates contributed the largest fraction of the sediment during the last week of the experiment as documented by a strong increase in biogenic silica fluxes (Fig. 7b), an elevated Si/C ratio (Fig. 7c) and microscopic inspection.

4 Discussion

4.1 Phase I

In the control treatments, dynamics in total inorganic carbon and gas exchange over the first 19 days of the experiment are well represented by measured production, export and respiration of particulate organic matter (Fig. 4a). Thus,

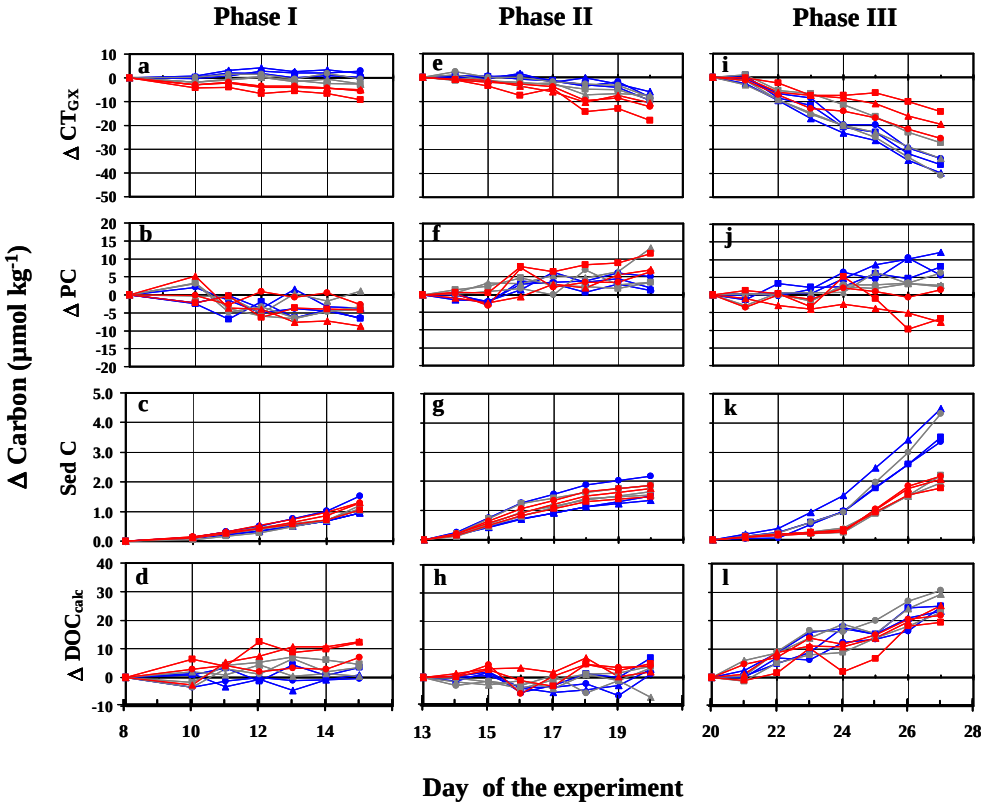

Fig. 6. Temporal development of carbon pools in all treatments for the three phases of the experiment. Biologically mediated changes in inorganic carbon concentrations (ΔCT_{GX}) together with changes in particulate carbon (ΔPC) and cumulative sedimentation of particulate carbon during each phase (Sed) were used to estimate dissolved organic carbon from mass balance ΔDOC_{calc}. CO_2 treatment levels and vertical dashed lines are coded as described for Fig. 3.

the carbon budget was closed with DOC_{calc} approaching zero at low CO_2. At high CO_2, however, there was significantly higher carbon consumption during phase I (Figs. 5c, 6a). Due to a strong vertical light gradient, ^{14}C gross primary production measured at 1 m water depth was high, showing a clear, positive correlation to CO_2 (Engel et al., 2013). In contrast, oxygen based production estimates by Tanaka et al. (2013) incubated at 3 m water depth were low and seem to be already partly balanced by respiration. The extra carbon ($\sim 13\,\mu mol\,kg^{-1}$) consumed at high CO_2 was not found in any of the particulate carbon pools (Fig. 6b, c), it was thus allocated to DOC_{calc}. Despite strong variability, statistical analyses of DOC measurements as well as ^{14}C DOC primary production measurements by Engel et al. (2013) support our interpretation of increased DOC production at high CO_2 in the phase before nutrient addition. DOC production was probably related to phytoplankton exudation but also to viral lyses of nanoplankton and microzooplankton grazing, both initiating the decline of the phase I bloom (Brussaard et al., 2013). Stronger microzooplankton grazing at low CO_2 during phase I was stated by de Kluijver et al. (2013) and Brussaard et al. (2013). Enhanced primary production at high CO_2 (Engel et al., 2013) presumably in combination with opposing strong heterotrophic loss processes at low CO_2 (Brussaard et al., 2013) were resulting in net uptake of inorganic carbon in the future CO_2 treatments and concomitant release of inorganic carbon in the low CO_2 controls (Fig. 6a). Rapid cycling of carbon during phase I obviously resulted in accumulation of DOC at high CO_2 that was not readily bioavailable and persisted at least during phase II, in which net production of DOC was considerably lower (Fig. 5f, see also Engel et al., 2013). A semi-labile nature of the produced dissolved organic matter in this experiment becomes also evident from apparent substrate limitation of heterotrophic bacteria during the entire experiment, detected by Piontek et al. (2013).

The phenomenon of inorganic carbon drawdown with low net consumption of N or P, called carbon over-consumption (Toggweiler, 1993), was enhanced at high CO_2 between t8 and t15. Such feature was already found in incubations of natural Atlantic plankton communities under high CO_2 (Schulz et al., 2008; Bellerby et al., 2008; Riebesell et al., 2007; Delille et al., 2005; Engel et al., 2004a; Egge et al., 2009; Hein and Sand-Jensen, 1997) and is also indicated by increased cumulative ^{14}C primary production observed during the experiment by Engel et al. (2013). The final product

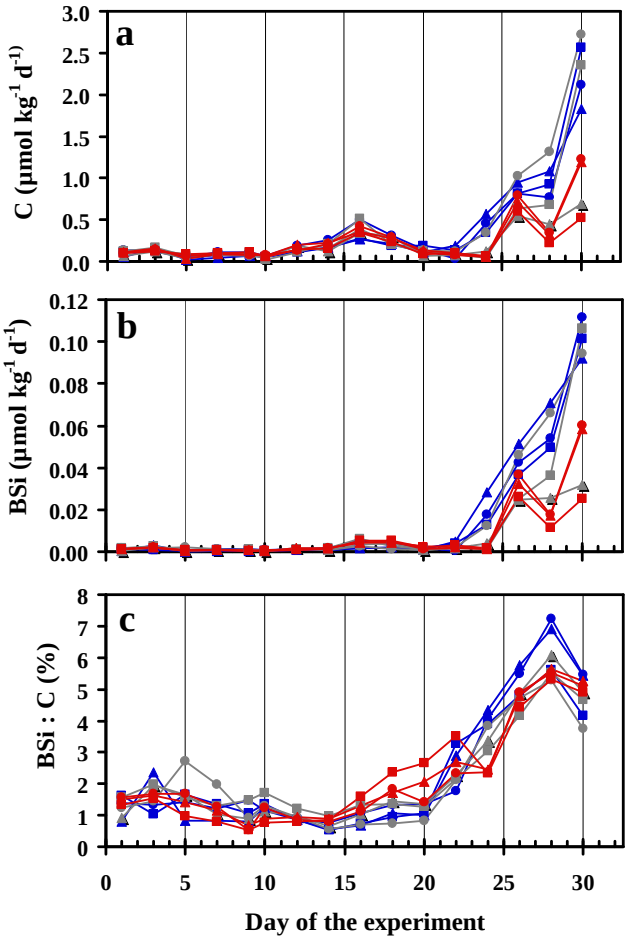

Fig. 7. Vertical fluxes for carbon **(a)** and biogenic silica **(b)** normalised to kg seawater and day. Biogenic silica to carbon ratios in the sedimented material are shown in **(c)**. Treatment levels and vertical dashed lines are coded as described for Fig. 3.

of enhanced photosynthetic activity could often not directly be measured, but was hypothesised to be released as DOC, subsequently occurring as TEP (Engel et al., 2004a). Sedimentation of aggregated DOC in the form of TEP was hypothesized to cause increased carbon loss under high CO_2 in the PEECE (Pelagic Ecosystem CO_2 Enrichment) III study (Schulz et al., 2008) and in further previous experiments (Engel et al., 2004b). In this experiment, an increased contribution of freshly fixed ^{13}C to high CO_2 sediments during phase I was argued to be caused by sinking of TEP by de Kluijver et al. (2013). TEP formation implies a flux of DOC into the PC pool, but neither increased bulk sedimentation nor increased carbon contents of sediments or of water-column particulate matter under high CO_2 were measured. Sediment fluxes were low and indication for TEP as a relevant aggregation factor was not detected. Sugars serving as precursors for TEP were possibly produced at concentrations too low to form relevant amounts of aggregates or were consumed by the bacterial community right after release (Piontek et al., 2010). DOC was therefore remaining in the water column, where it, on the long run, might support the development of the microbial community. Although an increase in bacterial numbers was not observed during the duration of the experiment (Brussaard et al., 2013), DOC accumulation rather promotes enhanced shallow remineralisation than primary production or export (Thingstad et al., 2008).

4.2 Phase II

During phase II the trends in uptake of inorganic C, N and P after nutrient addition were consistent with trends in Chl *a*. Elevated CO_2 concentrations seemed to have a stimulating effect on growth of the dominating picoeukaryotic primary producers (Brussaard et al., 2013; Schulz et al., 2013), leading to increased uptake of inorganic matter (Table 3, Fig. 6e), as well as increased cell numbers and Chl *a*. However, increasing biomass production as a result of enhanced nutrient uptake at high CO_2 during the bloom of picoeukaryotes in phase II was hardly detectable as particulate organic matter build-up and did not cause a significant sedimentation event (Figs. 6f, 5g). A peak in carbon export caused by Cirripedia larvae (t16, Fig. 7a) shows that the settling of meroplankton can seasonally account for a large portion of vertical fluxes in coastal ecosystems. This finding is in agreement with ^{13}C tracer data by de Kluijver et al. (2013). Generally low enrichment of sediment with the tracer during phases I and II can only be explained by high contents of zooplankton and "old" detrital material. Build-up of autotrophic biomass in the water column, estimated from Chl *a* as well as from biovolume of picoeukaryotes (Brussaard et al., 2013) can only account for the amount of inorganic C, N and P consumed during the first days of phase II. Thereafter, phytoplankton standing stocks were diminished and kept at a relatively low level by microzooplankton grazing and viral lyses of picoeucaryotes (Brussaard et al., 2013). Nutrient and carbon uptake continued during the time of strong biomass loss. Low C/N and C/P inorganic uptake ratios in all treatments suggest overall elevated production of organic P and N compared to organic C during phase II (Silyakova et al., 2012). Significant CO_2-correlated differences in ΔPC as well as ΔPOP_{calc} could not be detected during the entire phase II (Table 3). Dissolved organic matter is indeed showing positively CO_2-related differences in ΔDOC_{calc} (Fig. 6h) but also in ΔDOP. Release of cell contents rather than exudation may have been the source of this DOM at nutrient-replete conditions, as enhanced autotrophy at high CO_2 was strongly top–down controlled (Brussaard et al., 2013). In contrast to P and C, enhanced uptake of inorganic nitrogen at high CO_2 was also reflected in higher ΔPON and only minor amounts of N accumulated in DON_{calc}. Nitrogen was obviously preferentially incorporated into the heterotrophic community compared to C and P (Table 3).

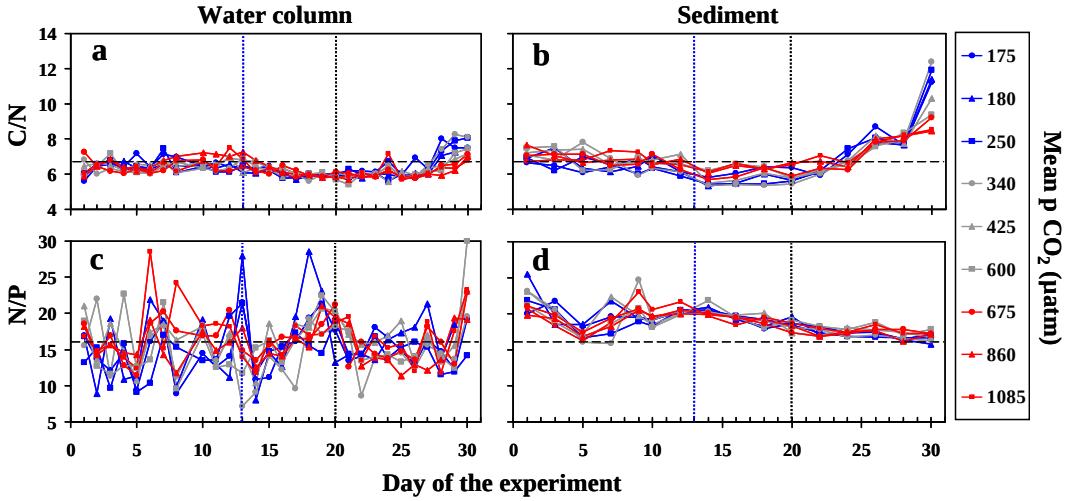

Fig. 8. Temporal development of measured carbon to nitrogen (C/N) and nitrogen to phosphorus (N/P) ratios of particles suspended in the water column (left) and particles sampled in the sediment traps (right). Dashed horizontal line marks Redfield ratios. CO_2 partial pressures given in the figure legend are mean values for the experiment (day 8–26). Vertical dashed lines are coded as described for Fig. 3.

4.3 Phase III

A relatively diverse phytoplankton community comprised of picoeukaryotes, co-dominated by diatoms and dinoflagellates established during phase III (Schulz et al., 2013; Brussaard et al., 2013). Biomass build-up resulting from fast carbon and nutrient drawdown did not seem to be limited by strong heterotrophic loss processes as observed in the previous two phases. This bloom showed higher C, N and P uptake rates at low CO_2, whereas under high CO_2 uptake was already slowing down due to nutrient depletion after the phase II peak (Fig. 6i). Reduced growth at high CO_2 in phase III was reflected by significantly lower ΔPC, ΔPON, and ΔPOP (Table 3). Diatoms, contributing relatively low biomass to the pelagic community (Schulz et al., 2013), increasingly dominated the sediment material from the beginning of phase III in all treatments. In the sediment material, this is illustrated by increasing BSi/C ratios from t20 onwards (Fig. 7c), concurring with microscopic observations of large quantities of diatom chains and their fatty acid signature detected by de Kluijver et al. (2013). Overall, higher biomass build-up seemed to be causing a sedimentation event of diatoms, forming aggregates with other particles, transporting them into the sediment trap. In contrast to the previous two phases, ^{13}C tracer concentrations indicate that there were even higher contributions of freshly fixed carbon to sediments than to water-column PC (de Kluijver et al., 2013). The retention food web, quickly recycling freshly produced biomass, seems to have shifted towards an export community in phase III (Wassmann, 1997). Strongly reduced export at high CO_2 was obviously due to nutrients being diminished by enhanced growth during phase II. Unfortunately, the total amount of export production cannot be calculated for this period, as measurements ended before peak sedimentation rates were reached (Fig. 7a). In addition to that, DOC_{calc} and wall-grown biomass, not being exported, were exponentially increasing (Fig. 4c). However, an export flux at high CO_2 comparable to fluxes observed at low CO_2 occurring after the end of our measurements (t30) seems unlikely, as inorganic N and P were depleted at t28. Until nutrient depletion, significantly less carbon uptake, PC and PON accumulation in the water column and less export of C, N and P were observed at high CO_2 during phase III.

4.4 Stoichiometry of exported particulate matter

Temporal trends in elemental composition of the sedimented particulate matter were very similar to that of the water column during most parts of the experiment (Fig. 8). Carbon isotope tracer data in sediments suggests that there was mostly an under-representation of phytoplankton biomass (de Kluiver et al., 2013). Elemental composition of sediment was overall similar to water column particulate matter. This classifies sinking material sampled at the bottom of the shallow mesocosms to be relativity fresh. Nevertheless, sinking detritus and digested material produced by the large heterotrophic community was probably responsible for the slight general offset in composition of sedimenting material towards higher C/N and N/P ratios throughout the experiment. While changes in particulate matter composition in response to future CO_2, reported from laboratory experiments on phytoplankton (Burkhardt et al., 1999; Burkhardt and Riebesell, 1997), are varying between species in strength and direction, differences in organic C/N/P ratios of primary producers growing under inorganic nutrient limitation and repletion are a common phenomenon (Klausmeier et al., 2004). The fact that we did not observe strong changes in response to nutrient or CO_2 addition, during this experiment is likely a

result of the diverse composition of POM, with phytoplankton comprising only a relatively small fraction during large parts of the experiment. Fast recycling of readily available N and P compounds during phase I were obviously covering the nutrient demand of phytoplankton (Schulz et al., 2013) and probably comprised a large part of the fluxes even during nutrient replete phases of the experiment.

The observed increase of C/N ratios in the sediment compared to the water-column particulate matter during phase III correlates with the occurrence of diatoms and increasing silicate flux (Fig. 7c). This diatom ballast or aggregation effect caused the over-representation of fresh carbon-rich particles in the sediments. The same C/N increase as in the sediment occurred later and less pronounced in the water column; here diatoms and fresh material are measured against a much larger background of other water-column particulate matter, thus diluting this signal.

On t30, higher C/N ratios at low CO_2 appeared in water-column particulate matter. Similar to the general increase of C/N in all mesocosms, also the CO_2 effect on C/N was amplified in the sediment. Mesocosms showing stronger elevated C/N ratios on the last day had also higher sedimentation rates of C, N, P and Si (Table 3). Carbon uptake beyond the day of nutrient depletion could not be determined, as the inorganic carbon dataset ends on t27. But already until t27 inorganic carbon to nutrient uptake was much higher at low CO_2 during phase III and thus even during the combined post nutrient phase (II + III) (Silyakova et al., 2012). A combination of high uptake rates and the shift towards increased C/N on the last days overcompensated initially higher uptake at high CO_2 during phase II. Elevated C or reduced N content of the phytoplankton community might have been due to growth limitation by dissolved inorganic nitrogen with concentrations below 1 µmol kg^{-1} (Klausmeier et al., 2004) already since t24 in all treatments.

4.5 Synthesis

Despite all efforts in determining all relevant elemental pools of C, N and P in regular temporal intervals, budgets could not readily be closed. This was mainly because of unsatisfying precision in DOC, DON and POP as well as wall growth towards the end of the experiment. However, gaps in the budget could be narrowed down by introducing novel methodology to determine gas exchange and sedimentation. It could be demonstrated that measured pools in large mesocosms can be quantitatively evaluated against each other. Moreover, using mass balance, problematic measurement parameters as well as technical and operational problems could be identified and their relevance could be quantified. In later experiments, improved sediment traps, an improved DOC sampling strategy as well as regular cleaning of the walls solved the most prominent problems pointed out in this study (see improved methods in Riebesell et al., 2013). The particular reason for the lack in precision in DON and POP within this dataset could not be ascertained.

Future CO_2 concentrations were found to stimulate autotrophic production twice during the course of this experiment. First during phase I, when increased inorganic carbon uptake by nanoplankton at high CO_2 was directly channelled into dissolved organics. Secondly, during phase II, when enhanced growth of picoeukaryotes diminished inorganic nutrient concentrations at high CO_2, resulting in less organic matter being exported in phase III. During this experiment, both positive effects on primary producers had negative influence on carbon export.

After phase I, community composition and carbon flows had changed. Later effects were therefore a product of complex resource competition and cascading loss processes modified by CO_2 and preceding production. The dominating producers or consumers in a mesocosm had responded to the manipulation at the beginning of the experiment, any following effects were multi-causal. Growth enhancement of nanoplankton and picoeukaryotes during phase I and II (Brussaard et al., 2013; Engel et al., 2013; de Kluiver et al., 2013) might have caused most of the CO_2 effects on bloom dynamics observed during and after their occurrence. Therefore, e.g. direct physiological CO_2 effects on plankton dominating within phase III would be a matter of speculation due to the different nutrient situation already in the beginning of phase III. This demonstrates that ecological data are of substantial importance in making biogeochemical response patterns comparable between experiments. Apparently, responses found for the retention type community, which was present at the start of this experiment, are not directly comparable to earlier findings for export systems such as the coccolithophore blooms in Norwegian coastal waters compiled by Riebesell et al. (2008). Community experiments always have to be seen as case studies with results primarily valid for the specific community composition enclosed at the start of the experiment. Further experiments will show whether CO_2 enhanced DOC production and growth of smaller phytoplankton can be consistently found at similar community composition.

Laboratory studies performed on single species are ideal to detect physiological CO_2 effects, whereas the importance of these effects within a natural ecosystem is always difficult to extrapolate (Riebesell and Tortell, 2011). In this experiment, ocean acidification/carbonation affected small phytoplankton, which in turn significantly influenced principle ecosystem functioning. Whereas enhanced growth of picoeucaryotes itself had no immediate effect on carbon export fluxes, their footprint in the nutrient budget controlled export fluxes later during the experiment. Identifying species that have the potential to change biogeochemical fluxes by influencing community succession is an important task for future mesocosm experiments. Focussing from the community to the species level instead of extrapolating from the laboratory

to the field could accelerate the progress of finding general biogeochemical response patterns.

Acknowledgements. This work is a contribution to the "European Project on Ocean Acidification" (EPOCA) which received funding from the European Community's Seventh Framework Programme (FP7/2007-2013) under grant agreement no. 211384. Financial support was provided through Transnational Access funds by the European Union Seventh Framework Program (FP7/2007-2013) under grant agreement no. 22822 MESOAQUA and by Federal Ministry of Education and Research (BMBF, FKZ 03F0608) through the BIOACID (Biological Impacts of Ocean ACIDification) project. We gratefully acknowledge the logistical support of Greenpeace International for its assistance with the transport of the mesocosm facility from Kiel to Ny-Ålesund and back to Kiel. We also thank the captains and crews of M/V *ESPERANZA* of Greenpeace and R/V *Viking Explorer* of the University Centre in Svalbard (UNIS) for assistance during mesocosm transport and during deployment and recovery in Kongsfjorden. We thank the staff of the French–German Arctic Research Base at Ny-Ålesund, in particular Marcus Schumacher, for on-site logistical support.

Edited by: J. Middelburg

The service charges for this open access publication have been covered by a Research Centre of the Helmholtz Association.

References

Bathmann, U. V., Noji, T. T., and von Bodungen, B.: Sedimentation of pteropods in the Norwegian Sea in autumn, Deep Sea Res., 38, 1341–1360, 1991.

Bellerby, R. G. J., Schulz, K. G., Riebesell, U., Neill, C., Nondal, G., Heegaard, E., Johannessen, T., and Brown, K. R.: Marine ecosystem community carbon and nutrient uptake stoichiometry under varying ocean acidification during the PeECE III experiment, Biogeosciences, 5, 1517–1527, doi:10.5194/bg-5-1517-2008, 2008.

Bellerby, R. G. J., Silyakova, A., Nondal, G., Slagstad, D., Czerny, J., de Lange, T., and Ludwig, A.: Marine carbonate system evolution during the EPOCA Arctic pelagic ecosystem experiment in the context of simulated Arctic ocean acidification, Biogeosciences Discuss., 9, 15541–15565, doi:10.5194/bgd-9-15541-2012, 2012.

Bopp, L., Monfray, P., Aumont, O., Dufresne, J.-L., Le Treut, H., Madec, G., Terray, L., and Orr, J. C.: Potential impact of climate change on marine export production. Global Biogeochem. Cy., 15, 81–99. 2001.

Brussaard, C. P. D., Noordeloos, A. A. M., Witte, H., Collenteur, M. C. J., Schulz, K., Ludwig, A., and Riebesell, U.: Arctic microbial community dynamics influenced by elevated CO_2 levels, Biogeosciences, 10, 719–731, doi:10.5194/bg-10-719-2013, 2013.

Burkhardt, S. and Riebesell, U.: CO_2 availability affects elemental composition (C : N : P) of the marine diatom *Skeletonema costatum*, Mar. Ecol.-Prog. Ser., 155, 67–76, doi:10.3354/meps155067, 1997.

Burkhardt, S., Zondervan, I., and Riebesell, U.: Effect of CO_2 concentration on the C : N : P ratio in marine phytoplankton: A species comparison., Limnol. Oceanogr., 44, 683–690, 1999.

Comeau, S., Gorsky, G., Jeffree, R., Teyssié, J.-L., and Gattuso, J.-P.: Impact of ocean acidification on a key Arctic pelagic mollusc (*Limacina helicina*), Biogeosciences, 6, 1877–1882, doi:10.5194/bg-6-1877-2009, 2009.

Czerny, J., Schulz, K. G., Krug, S. A., Ludwig, A., and Riebesell, U.: Technical Note: The determination of enclosed water volume in large flexible-wall mesocosms "KOSMOS", Biogeosciences, 10, 1937–1941, doi:10.5194/bg-10-1937-2013, 2013a.

Czerny, J., Schulz, K. G., Ludwig, A., and Riebesell, U.: Technical Note: A simple method for air–sea gas exchange measurements in mesocosms and its application in carbon budgeting, Biogeosciences, 10, 1379–1390, doi:10.5194/bg-10-1379-2013, 2013b.

de Kluijver, A., Soetaert, K., Czerny, J., Schulz, K. G., Boxhammer, T., Riebesell, U., and Middelburg, J. J.: A ^{13}C labelling study on carbon fluxes in Arctic plankton communities under elevated CO_2 levels, Biogeosciences, 10, 1425–1440, doi:10.5194/bg-10-1425-2013, 2013.

Delille, B., Harlay, J., Zondervan, I., Jacquet, S., Chou, L., Wollast, R., Bellerby, R. G. J., Frankignoulle, M., Borges, A. V., Riebesell, U., and Gattuso, J.-P.: Response of primary production and calcification to changes of pCO_2 during experimental blooms of the coccolithophorid Emiliania huxleyi, Global Biogeochem. Cy., 19, GB2023, doi:10.1029/2004gb002318, 2005.

Doney, S. C.: The Growing Human Footprint on Coastal and Open-Ocean Biogeochemistry, Science, 328, 1512–1516, doi:10.1126/science.1185198, 2010.

Egge, J. K., Thingstad, T. F., Larsen, A., Engel, A., Wohlers, J., Bellerby, R. G. J., and Riebesell, U.: Primary production during nutrient-induced blooms at elevated CO_2 concentrations, Biogeosciences, 6, 877–885, doi:10.5194/bg-6-877-2009, 2009.

Engel, A.: Direct relationship between CO_2 uptake and transparent exopolymer particles production in natural phytoplankton, J. Plankton Res., 24, 49–53, 2002.

Engel, A., Delille, B., Jacquet, S., Riebesell, U., Rochelle-Newall, E., Terbrüggen, A., and Zondervan, I.: Transparent exopolymer particles and dissolved organic carbon production by Emiliania huxleyi exposed to different CO_2 concentrations: a mesocosm experiment, Limnol. Oceanogr, 50, 493–507, 2004a.

Engel, A., Thoms, S., Riebesell, U., Rochelle-Newall, E., and Zondervan, I.: Polysaccharide aggregation as a potential sink of marine dissolved organic carbon, Nature, 428, 929–932, 2004b.

Engel, A., Borchard, C., Piontek, J., Schulz, K. G., Riebesell, U., and Bellerby, R.: CO_2 increases ^{14}C primary production in an Arctic plankton community, Biogeosciences, 10, 1291–1308, doi:10.5194/bg-10-1291-2013, 2013.

Fabry, V. J., Seibel, B. A., Feely, R. A., and Orr, J. C.: Impacts of ocean acidification on marine fauna and ecosystem processes, ICES J. Mar. Sci., 65, 414–432, doi:10.1093/icesjms/fsn048, 2008.

Friedlingstein, P., Houghton, R. A., Marland, G., Hackler, J., Boden, T. A., Conway, T. J., Canadell, J. G., Raupach, M. R., Ciais, P., and Le Quéré, C.: Update on CO_2 emissions, Nat. Geosci, 3, 811–812, 2010.

Grasshoff, K., Ehrhardt, M., and Kremling., K.: Methods of Seawater Analysis., 2 Edn., Verlag Chemie, Weinheim, Germany, 1983.

Gruber, N.: Warming up, turning sour, losing breath: ocean biogeochemistry under global change, Philos. T. Roy. Soc. A, 369, 1980–1996, doi:10.1098/rsta.2011.0003, 2011.

Hansen, H. and Koroleff, R.: in: Methods of Seawater Analysis, edited by: Grasshoff, K., Kremmling, K., and Ehrhardt, M., Wiley, Weinheim, Germany, 159–228, 1999.

Hansen, J., Sato, M., Ruedy, R., Lo, K., Lea, D. W., and Medina-Elizade, M.: Global temperature change, P. Natl. Acad. Sci. USA, 103, 14288–14293, doi:10.1073/pnas.0606291103, 2006.

Hein, M. and Sand-Jensen, K.: CO_2 increases oceanic primary production, Nature, 388, 526–527, 1997.

Holmes, R. M., Aminot, A., Kerouel, R., Hooker, B. A., and Peterson, B. J.: A simple and precise method for measuring ammonium in marine and freshwater ecosystems, Can. J. Fish. Aquat. Sci., 56, 1801–1808, doi:10.1139/f99-128, 1999.

Hoover, T. E. and Berkshire, D. C.: Effects of Hydration on Carbon Dioxide Exchange across an Air-Water Interface, J. Geophys. Res., 74, 456–464, doi:10.1029/JB074i002p00456, 1969.

Klaas, C. and Archer, D. E.: Association of sinking organic matter with various types of mineral ballast in the deep sea: Implications for the rain ratio, Global Biogeochem. Cy., 16, 1116, doi:10.1029/2001gb001765, 2002.

Klausmeier, C., Litchman, E., and Levin, S.: Phytoplankton growth and stoichiometry under multiple nutrient limitation, Limnol. Oceanogr., 49, 1463–1470, 2004.

Lewis, E. and Wallace, D. W. R.: Program developed for CO_2 system calculations. ORNL/CDIAC-105. Carbon Dioxide Information Center, Oak Ridge National Laboratory, US Department of Energy, Oak Ridge, Tennessee, 1998.

Li, Q. P., Franks, P. J. S., Landry, M. R., Goericke, R., and Taylor, A. G.: Modeling phytoplankton growth rates and chlorophyll to carbon ratios in California coastal and pelagic ecosystems, J. Geophys. Res., 115, G04003, doi:10.1029/2009jg001111, 2010.

Lischka, S., Büdenbender, J., Boxhammer, T., and Riebesell, U.: Impact of ocean acidification and elevated temperatures on early juveniles of the polar shelled pteropod *Limacina helicina*: mortality, shell degradation, and shell growth, Biogeosciences, 8, 919–932, doi:10.5194/bg-8-919-2011, 2011.

Lombard, F., da Rocha, R. E., Bijma, J., and Gattuso, J.-P.: Effect of carbonate ion concentration and irradiance on calcification in planktonic foraminifera, Biogeosciences, 7, 247–255, doi:10.5194/bg-7-247-2010, 2010.

Lutz, M. J., Caldeira, K., Dunbar, R. B., and Behrenfeld, M. J.: Seasonal rhythms of net primary production and particulate organic carbon flux to depth describe the efficiency of biological pump in the global ocean, J. Geophys. Res., 112, C10011, doi:10.1029/2006jc003706, 2007.

Meehl, G. A. S., T. F., Collins, W. D., Friedlingstein, A. T., Gaye, A. T., Gregory, J. M., Kitoh, A., Knutti, R., Murphy, J. M., Noda, A., Raper, S. C. B., Watterson, I. G., Weaver, A. J., and Zhao, Z.: Global climate projections., in: Climate Change 2007, The physical science basis, edited by: Solomon, S., Qin, D., and Manning, M., Technical support unit, IPCC working group 1, Cambridge University Press, 748–845, 2007.

Millero, F. J., Woosley, R., DiTrolio, B., and Waters, J.: Effect of Ocean Acidification on the Speciation of Metals in Seawater, Oceanography, 22, 72–85, 2009.

Niehoff, B., Schmithüsen, T., Knüppel, N., Daase, M., Czerny, J., and Boxhammer, T.: Mesozooplankton community development at elevated CO_2 concentrations: results from a mesocosm experiment in an Arctic fjord, Biogeosciences, 10, 1391–1406, doi:10.5194/bg-10-1391-2013, 2013.

Oschlies, A.: Impact of atmospheric and terrestrial CO_2 feedbacks on fertilization-induced marine carbon uptake, Biogeosciences, 6, 1603–1613, doi:10.5194/bg-6-1603-2009, 2009.

Petit, J. R., Jouzel, J., Raynaud, D., Barkov, N. I., Barnola, J.-M., Basile, I., Bender, M., Chappellaz, J., Davis, M., Delaygue, G., Delmotte, M., Kotlyakov, V. M., Legrand, M., Lipenkov, V. Y., Lorius, C., P.Épin, L., Ritz, C., Saltzman, E., and Stievenard., M.: Climate and atmospheric history of the past 420,000 years from the Vostok ice core, Antarctica, Nature, 399, 429–436 1999.

Piontek, J., Lunau, M., Händel, N., Borchard, C., Wurst, M., and Engel, A.: Acidification increases microbial polysaccharide degradation in the ocean, Biogeosciences, 7, 1615–1624, doi:10.5194/bg-7-1615-2010, 2010.

Piontek, J., Borchard, C., Sperling, M., Schulz, K. G., Riebesell, U., and Engel, A.: Response of bacterioplankton activity in an Arctic fjord system to elevated pCO_2: results from a mesocosm perturbation study, Biogeosciences, 10, 297–314, doi:10.5194/bg-10-297-2013, 2013.

Qian, J. and Mopper, K.: Automated High-Performance, High-Temperature Combustion Total Organic Carbon Analyzer, Anal. Chem., 68, 3090–3097, doi:10.1021/ac960370z, 1996.

Reinfelder, J. R.: Carbon Concentrating Mechanisms in Eukaryotic Marine Phytoplankton, Annual Review of Marine Science, 3, 291–315, doi:10.1146/annurev-marine-120709-142720, 2011.

Revelle, R. and Suess, H. E.: Carbon Dioxide Exchange Between Atmosphere and Ocean and the Question of an Increase of Atmospheric CO_2 during the Past Decades, Tellus, 9, 18–27, doi:10.1111/j.2153-3490.1957.tb01849.x, 1957.

Riebesell, U.: Effects of CO_2 Enrichment on Marine Phytoplankton, J. Oceanogr., 60, 719–729, doi:10.1007/s10872-004-5764-z, 2004.

Riebesell, U. and Tortell, P. D.: Effects of ocean acidification on pelagic organisms and ecosystems, in: Ocean Acidification, edited by: Gattuso, J. P. and Hanson, L., Oxford University Press, Oxford, 99–121, 2011.

Riebesell, U., Schulz, K. G., Bellerby, R. G., Botros, M., Fritsche, P., Meyerhöfer, M., Neill, C., Nondal, G., Oschlies, A., Wohlers, J., and Zöllner., E.: Enhanced biological carbon consumption in a high CO_2 ocean, Nature, 450, 545–548, 2007.

Riebesell, U., Bellerby, R. G. J., Grossart, H.-P., and Thingstad, F.: Mesocosm CO_2 perturbation studies: from organism to community level, Biogeosciences, 5, 1157–1164, doi:10.5194/bg-5-1157-2008, 2008.

Riebesell, U., Körtzinger, A., and Oschlies, A.: Sensitivities of marine carbon fluxes to ocean change, P. Natl. Acad. Sci. USA, 106, 20602–20609, doi:10.1073/pnas.0813291106, 2009.

Riebesell, U., Czerny, J., von Bröckel, K., Boxhammer, T., Büdenbender, J., Deckelnick, M., Fischer, M., Hoffmann, D., Krug, S. A., Lentz, U., Ludwig, A., Muche, R., and Schulz, K. G.: Technical Note: A mobile sea-going mesocosm system – new opportunities for ocean change research, Biogeosciences, 10, 1835–1847, doi:10.5194/bg-10-1835-2013, 2013.

Sabine, C. L., Feely, R. A., Gruber, N., Key, R. M., Lee, K., Bullister, J. L., Wanninkhof, R., Wong, C. S., Wallace, D. W. R., Tilbrook, B., Millero, F. J., Peng, T.-H., Kozyr, A., Ono, T., and Rios, A. F.: The Oceanic Sink for Anthropogenic CO_2, Science,

305, 367–371, doi:10.1126/science.1097403, 2004.

Sarmiento, J. L. and Le Quéré, C.: Oceanic Carbon Dioxide Uptake in a Model of Century-Scale Global Warming, Science, 274, 1346–1350, doi:10.1126/science.274.5291.1346, 1996.

Sarmiento, J. L., Slater, R., Barber, R., Bopp, L., Doney, S. C., Hirst, A. C., Kleypas, J., Matear, R., Mikolajewicz, U., Monfray, P., Soldatov, V., Spall, S. A., and Stouffer, R.: Response of ocean ecosystems to climate warming, Global Biogeochem. Cy., 18, GB3003, doi:10.1029/2003GB002134, 2004.

Schmittner, A., Oschlies, A., Matthews, H. D., and Galbraith, E. D.: Future changes in climate, ocean circulation, ecosystems, and biogeochemical cycling simulated for a business-as-usual CO_2 emission scenario until year 4000 AD, Global Biogeochem. Cy., 22, GB1013, doi:10.1029/2007gb002953, 2008.

Schulz, K. G., Riebesell, U., Bellerby, R. G. J., Biswas, H., Meyerhöfer, M., Müller, M. N., Egge, J. K., Nejstgaard, J. C., Neill, C., Wohlers, J., and Zöllner, E.: Build-up and decline of organic matter during PeECE III, Biogeosciences, 5, 707–718, doi:10.5194/bg-5-707-2008, 2008.

Schulz, K. G., Bellerby, R. G. J., Brussaard, C. P. D., Büdenbender, J., Czerny, J., Engel, A., Fischer, M., Koch-Klavsen, S., Krug, S. A., Lischka, S., Ludwig, A., Meyerhöfer, M., Nondal, G., Silyakova, A., Stuhr, A., and Riebesell, U.: Temporal biomass dynamics of an Arctic plankton bloom in response to increasing levels of atmospheric carbon dioxide, Biogeosciences, 10, 161–180, doi:10.5194/bg-10-161-2013, 2013.

Sharp, J. H.: Improved analysis for "particulate" organic carbon and nitrogen from seawater, Limnol. Oceanogr., 19, 984–989, 1974.

Silyakova, A., Bellerby, R. G. J., Czerny, J., Schulz, K. G., Nondal, G., Tanaka, T., Engel, A., De Lange, T., and Riebesell, U.: Net community production and stoichiometry of nutrient consumption in a pelagic ecosystem of a northern high latitude fjord: mesocosm CO_2 perturbation study, Biogeosciences Discuss., 9, 11705–11737, doi:10.5194/bgd-9-11705-2012, 2012.

Tanaka, T., Alliouane, S., Bellerby, R. G. B., Czerny, J., de Kluijver, A., Riebesell, U., Schulz, K. G., Silyakova, A., and Gattuso, J.-P.: Effect of increased pCO_2 on the planktonic metabolic balance during a mesocosm experiment in an Arctic fjord, Biogeosciences, 10, 315–325, doi:10.5194/bg-10-315-2013, 2013.

Thingstad, T. F., Bellerby, R. G. J., Bratbak, G., Borsheim, K. Y., Egge, J. K., Heldal, M., Larsen, A., Neill, C., Nejstgaard, J., Norland, S., Sandaa, R. A., Skjoldal, E. F., Tanaka, T., Thyrhaug, R., and Topper, B.: Counterintuitive carbon-to-nutrient coupling in an Arctic pelagic ecosystem, Nature, 455, 387–390, 2008.

Toggweiler, J. R.: Carbon overconsumption, Nature, 363, 210–211, 1993.

Volk, T. and Hoffert, M. I.: Ocean carbon pumps – Analyses of reactive strengths and efficiencies in ocean-driven atmospheric CO_2 changes, in: The Carbon Cycle and Atmospheric CO_2: Natural Variations, Archean to Present, edited by: Sundquist, E. and Broecker, W., AGU Geophysical Monograph, Washington DC, 99–110, 1985.

von Bodungen, B., Antia, A., Bauerfeind, E., Haupt, O., Koeve, W., Machado, E., Peeken, I., Peinert, R., Reitmeier, S., Thomsen, C., Voss, M., Wunsch, M., Zeller, U., and Zeitzschel, B.: Pelagic processes and vertical flux of particles: an overview of a long-term comparative study in the Norwegian Sea and Greenland Sea, Geol. Rundsch., 84, 11–27, doi:10.1007/bf00192239, 1995.

Wassmann, P.: Retention versus export food chains: processes controlling sinking loss from marine pelagic systems, Hydrobiologia, 363, 29–57, 10.1023/a:1003113403096, 1997.

Welschmeyer, N. A.: Fluorometric analysis of chlorophyll a in the presence of chlorophyll b and pheopigments, Limnol. Oceanogr., 29, 1985–1992, 1994.